

BEHAVIOR OF COMPOSITE CFT BEAM-COLUMNS BASED ON NONLINEAR FIBER ELEMENT ANALYSIS

Tiziano Perea
Georgia Institute of Technology
Atlanta, GA 30332-0355
Email: tperea@gatech.edu

Roberto Leon
Georgia Institute of Technology
Atlanta, GA 30332-0355
Email: roberto.leon@ce.gatech.edu

Abstract

The results obtained from nonlinear fiber element analyses for concrete filled tubes (CFT) are discussed. The studies were aimed at assessing primarily the overall behavior and stability effects on these structural elements as a prelude to a large full-scale testing program. The study focuses on ultimate strength analyses for CFT composite columns with different stress-strain models for both concrete and steel. Fiber analyses using OpenSees are used to assess the impact on the ultimate strength based on the assumed stress-strain material curves, member slenderness, initial imperfections, and both material and geometric nonlinearities. Fiber analysis results are also compared with those obtained from AISC (2005). Fiber-based results show a compatible correlation with the expected element behavior, which is also captured in the current AISC (2005) Specifications.

Introduction

The use of composite columns in moment-resistance frame systems is increasing worldwide. Composite columns not only provide many advantages in construction speed and economy, but also result in a substantial improvement of mechanical properties of the member when compared to either steel or reinforced concrete columns. However, there still exist some knowledge gaps in their behavior in areas such as the effective stiffness under lateral forces, instability effects in slender beam-columns, and the secondary effects due to the steel-concrete contact interaction. Nonlinear fiber element analyses provide a very useful analytical tool to investigate some of these behavioral aspects of composite elements. Fiber elements offer an efficient approach as they can incorporate directly into the model flexural buckling, initial imperfection, geometric and material nonlinearity, and hardening effects.

Fiber element analysis have been widely used to understand and predict the behavior of steel (i.e. White, 1986; Liew and Chen 2004; etc.), reinforced concrete (i.e. Taucer et al., 1991; Izzudin et al., 1993; Spacone and Filippou, 1995; etc.) and composite steel-concrete elements. Table 1 summarizes briefly a number of analytical studies that have looked at fiber analysis of composite elements; this table is not meant to be comprehensive, however it gives an idea of the maturity and breath of the approach.

Table 1. Summary of analytical studies with fiber analysis in composite elements

Reference	Applied to:	Brief comments
Tomii and Sakino (1979)	CCFT and RCFT cross-sections	Calibrated fiber $M-\phi$ results with experimental results adjusting $\sigma-\varepsilon$ curve in concrete, keeping steel as elastic-perfectly-plastic.
Elnashai and Elghazouli (1993)	SRC beam-columns	Developed a non-linear model for SRC frame structures subjected to cyclic and dynamic loads, accounting for geometric nonlinearities, material inelasticity, confinement effects in concrete, and local buckling and cyclic degradation in the steel. The model is calibrated and compared with experimental data.
Ricles and Paboojian (1994)	SRC beam-columns	Analyzed SRC beam-columns with fiber analysis, which accounted for strain compatibility, material nonlinearity, and confinement effects using the Mander model.
Hajjar and Gourley (1996)	RCFT cross-sections	Developed a polynomial expression to represent a 3D axial-bending interaction equation for square CFT cross-sections. This polynomial equation was fitted based on results from nonlinear fiber element analysis.
EI-Tawil and Dierlein (1999)	SRC cross-sections	Compared experimental and fiber-based results of monotonic $M-\phi$ curves. From the fiber-based model, interaction curves were obtained for 3 SRC cross-sections with different steel ratios, which were compared with the ACI and AISC strength.
Lakshimi and Shanmugan (2000)	CFT beam-columns	Used fiber models to predict behavior of biaxially-loaded CFT beam-columns and axially-loaded slender CFT columns.
Uy (2000)	CFT columns	Used fiber models in CFT columns with thin-walled steel tubes. Buckling and post-buckling behavior were incorporated through a finite strip method and an effective width approach.
Aval et al. (2002)	CCFT and RCFT beam-columns	Developed a fiber element accounting for bond/slip interaction between concrete and steel (due to the difference between axial elongation and curvatures). The effect of semi- and perfect bond is investigated and compared with experiments.
Fujimoto et al. (2004)	RCFT cross-sections	Used the empirical $\sigma-\varepsilon$ curves developed by Nakahara-Sakino-Inai in fiber analysis to predict monotonic $M-\phi$ curves.
Inai et al. (2004)	RCFT cross-sections	Used the empirical $\sigma-\varepsilon$ curves developed by Nakahara-Sakino-Inai in fiber analysis to predict cyclic $M-\phi$ curves.
Varma et al. (2004)	RCFT beam-columns	Adapted and implemented $\sigma-\varepsilon$ curves for both high strength steel and concrete to predict the response of square CFT elements. These curves were adapted from results of 3D finite element analyses, which implicitly accounts for local buckling of the steel tube, transverse interaction between steel and concrete infill, and confinement of the concrete infill.
Lu et al. (2006)	RCFT cross-sections	Obtained $M-\phi$ curves and interaction $P-M_u$ diagrams, which accounted for residual stresses in the steel and confinement effects in concrete, as well as the material nonlinearity.
Choi et al. (2006)	RCFT cross-sections	Developed a parametric study to determine the P-M interaction diagram varying with the b/t and f_c'/F_y ratios.
Kim and Kim (2006)	RCFT beam-columns	Compared fiber-based cyclic $M-\phi$ and force-displacement ($F-\Delta$) curves with those obtained experimentally.
Liang (2008)	RCFT cross-sections	Determined P-M interaction diagrams for short CFT beam-columns assuming material nonlinearity. Fiber element results are compared with experimental data and existing solutions. Evaluated the influence of steel ratios, f_c' and F_y .

The results shown in this paper were aimed at assessing primarily the overall behavior and stability effects on composite CFT structural elements as a prelude to a large full-scale testing program. Fiber analysis results were obtained with the software OpenSees (Makena and Fenves, 1999), which confinement effects, local buckling, member slenderness and instability effects are being predicted.

An overview of nonlinear fiber element analysis

Fiber element analysis is a numerical technique which models a structural element by dividing it into a number of two-end frame elements, and by linking each boundary to a discrete cross-section with a grid of fibers (Figure 1). The material stress-strain response in each fiber is integrated to get stress-resultant forces and rigidity terms, and from these, forces and rigidities over the length are obtained through finite element interpolation functions which must satisfy equilibrium and compatibility conditions.

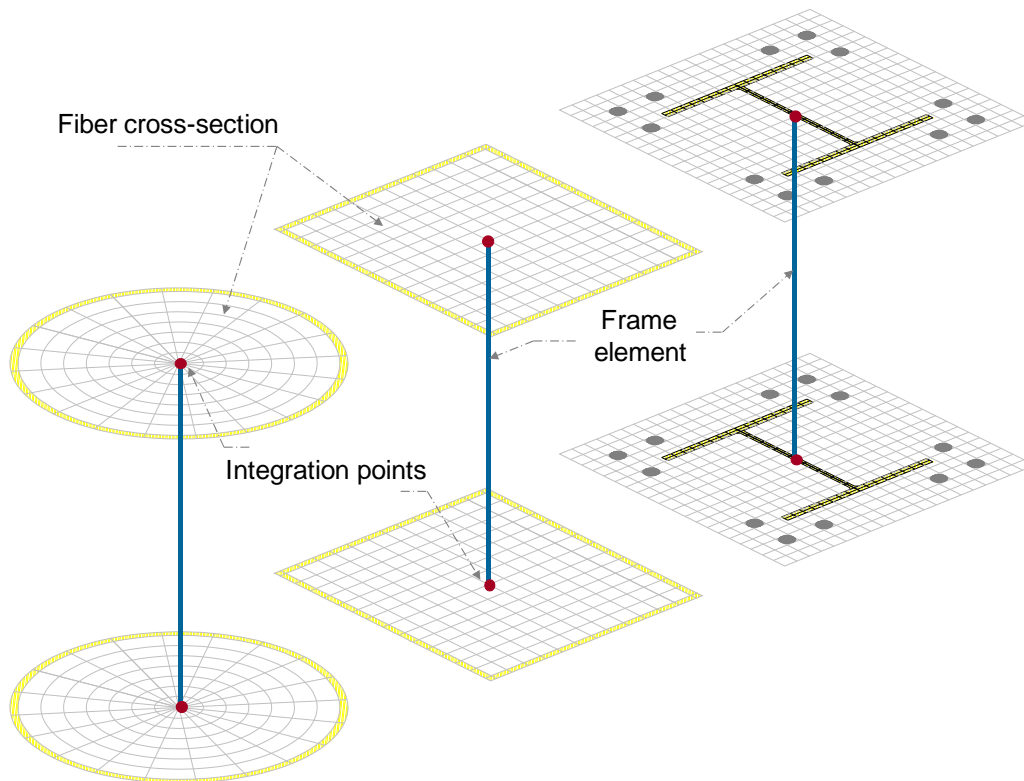


Figure 1. Frame element with ends coupled to fiber cross-sections

There are several advantages which justify the use of fiber analysis. Some of these advantages include but are not limited to their ability to handle:

- Complex cross-sections. A fiber cross-section can have any general geometric configuration formed by subregions of simpler shapes; geometric properties of the more complex section are calculated through the numerical integration.
- Tapered elements. Since the length of the fiber is not considered, the cross-section defined at each of the two ends can be different, and therefore, the response can be roughly estimated. Precision can be increased with more integration points.
- Complex strength-strain behavior. Since each fiber can have any stress-strain response, this technique allows modeling nonlinear behavior in steel members (steel σ - ϵ and residual stresses), reinforced concrete members (unconfined and confined concrete σ - ϵ , and steel reinforced σ - ϵ), and composite members.
- Accuracy and efficiency. Since each fiber is associated to a given uniaxial stress-strain (σ - ϵ) material response, higher accuracy and more realistic behavior effects can be captured in a fiber-based model than in a frame-based model, and at less computing time than for a 3D finite-based model.

As described previously, the uniaxial σ - ε curve can directly account for the material nonlinearity in monotonic or cyclic loads or displacements, and the residual stresses in the structural steel members. However, some researchers have calibrated, based on experimental or analytical 3D finite-based results (i.e. Varma et al., 2004; Tort and Hajjar, 2007), the uniaxial σ - ε to account for additional behavior effects like:

- Confinement effects in the concrete due to either steel reinforcement (as in RC or SRC cross-sections) or a steel tube (as in CFT cross-sections). Concrete confinement in CFT elements remain meanwhile the steel-concrete contact is hold.
- Local buckling in steel tubes through a degradation of the compressive σ - ε beyond the corresponding strain (ε_{lb}) when local buckling take place. Local buckling in CFT elements can be reached when the steel is highly stressed and the steel-concrete contact is lost.

Stability effects through geometric nonlinearity and initial imperfections can be captured directly with the frame-based analysis. In turn, slip between concrete and steel have been modeled in the frame-based formulation by adding degrees-of-freedom (i.e. Hajjar et al., 1998, Aval et al., 2002; Tort and Hajjar, 2007).

Stress-strain modeling

Fiber analyses are obviously sensitive to the assumptions in the stress-strain curves. Consequently, several research studies have been conducted on this topic to predict more “realistic” responses.

The current AISC (2005) specification allows the use of strain compatibility and fully-plastic stress distribution methods to calculate the cross-section strength. The plastic distribution method (Roik and Bergmann, 1992) basically assumes that each component in cross-section has reached the maximum plastic stress (Figure 2).

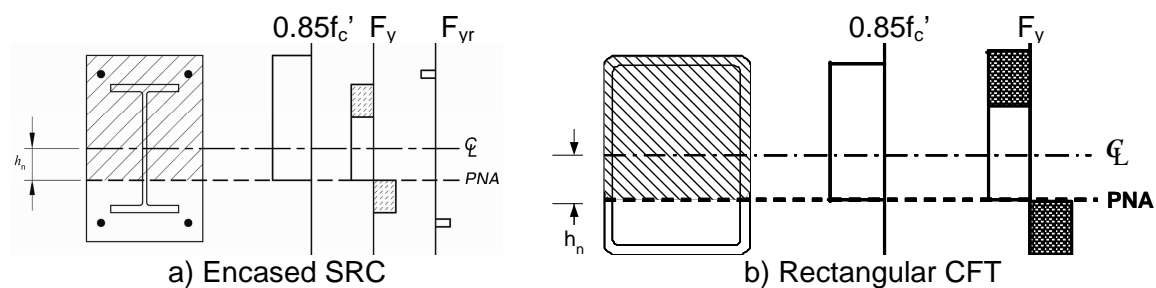


Figure 2. Fully-plastic stress distribution in composite cross-sections

While very useful and accurate for design purposes, the plastic distribution approach can only match the ultimate strength of the cross-section. When the entire moment-curvature (or load-deformation) behavior is of interests, more complex uniaxial stress-strain curves are needed. These include strain compatibility approaches to model reinforced concrete (i.e. Kent and Park, 1971; Mander et. al., 1988), steel (i.e. Menegotto and Pinto, 1973), CFT (i.e. Collins and Mitchell, 1990; Sakino and Sun, 1994; Chang and Mander, 1994; Nakahara and Sakino, 1998; Susantha et al., 2001), and SRC members (similar to those used for RC and steel).

The concrete model proposed by Kent and Park (1971) is defined by a curve up to the peak strength (Equation 1) followed by a descending line and finally constant beyond

some residual stress (f_{cr}) and strain (ε_{cr}); the values f_c' and $\varepsilon_c=2f_c'/E_c$ used in this equation for plain concrete are replaced by f_{cc}' and ε_{cc} in confined concrete (Figure 3.a).

$$\sigma(\varepsilon) = f_c' \left(\frac{2\varepsilon}{\varepsilon_c} - \left(\frac{\varepsilon}{\varepsilon_c} \right)^2 \right) \quad (1)$$

The concrete model proposed by Popovics (1973) is a continuous σ - ε curve in terms of the peak strength and an empirical coefficient $n=E_c/(E_c-f_c'/\varepsilon_c)$. Based on this equation, Mander *et al.* (1988) proposed an approach to estimate the confinement parameters f_{cc}' , ε_{cc} , ε_{cu} that best fit the σ - ε response of rectangular and circular reinforced concrete columns confined by stirrups and spirals (Equation 2, Figure 3.b).

$$\sigma(\varepsilon) = f_{cc}' \left(\frac{\varepsilon}{\varepsilon_{cc}} \right) \left(\frac{n}{n-1 + (\varepsilon/\varepsilon_{cc})^n} \right) \quad (2)$$

$$\varepsilon_{cc} = \varepsilon_c \left[1 + 5 \left(\frac{f_{cc}'}{f_c'} - 1 \right) \right]$$

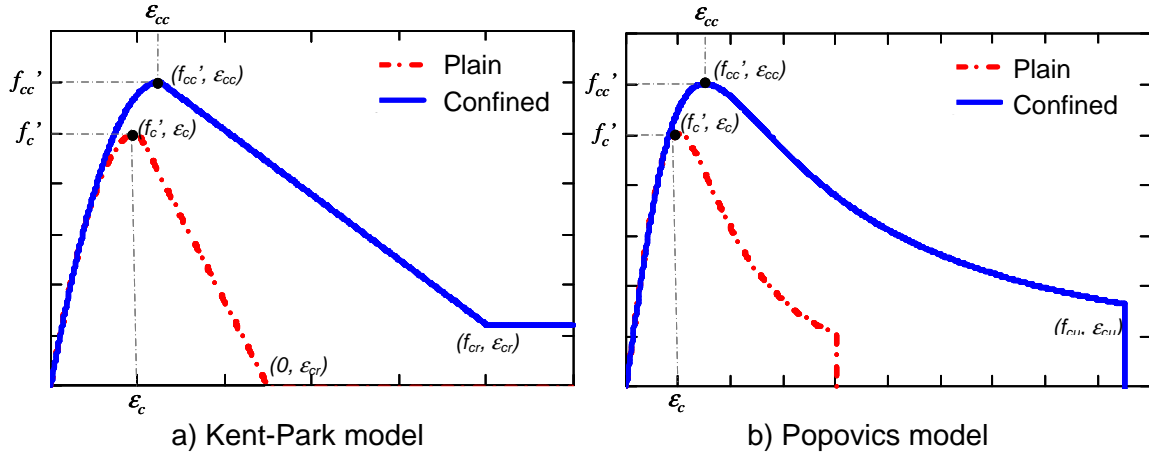


Figure 3. σ - ε curves in plain and confined concrete

Based on empirical data and its calibration with an analytical study, Sakino and Sun (1994) proposed uniaxial σ - ε models for both concrete (Equation 3, Figure 4) and steel (Figure 5) for circular and rectangular CFT elements that account for confinement, local buckling and biaxial stresses. Equation 3 describes the σ - ε curve for concrete proposed by Sakino and Sun (1994), which is in terms of the effective hoop stresses (σ_{re}) and the peak concrete strength.

$$\sigma(\varepsilon) = f_{cc}' \left(\frac{V(\varepsilon/\varepsilon_{cc}) + (W-1)(\varepsilon/\varepsilon_{cc})^2}{1 + (V-2)(\varepsilon/\varepsilon_{cc}) + W(\varepsilon/\varepsilon_{cc})^2} \right) \quad (3)$$

Where: $V = \frac{E_c \varepsilon_{cc}}{f_{cc}'}$ $W = 1.5 - 0.0171 f_c' (MPa) + 2.39 \sqrt{\sigma_{re} (MPa)}$ (3.a)

And the effective hoop stresses (σ_{re}) and the peak strength values are defined by:
 For circular CFTs:

$$\sigma_{re} = \frac{0.0677F_y}{D/t-2}$$

$$f_{cc}' = f_c' + \frac{1.558F_y}{D/t-2}$$

$$\varepsilon_{cc} = \begin{cases} \varepsilon_c \left[1 + 4.7 \left(\frac{f_{cc}'}{f_c'} - 1 \right) \right] & \text{if } f_{cc}' < 1.5f_c' \\ \varepsilon_c \left[3.35 + 20 \left(\frac{f_{cc}'}{f_c'} - 1.5 \right) \right] & \text{if } f_{cc}' \geq 1.5f_c' \end{cases}$$

For rectangular CFTs:

$$\sigma_{re} = \frac{2(b/t-1)F_y}{(b/t-2)^3}$$

$$f_{cc}' = f_c' \quad (3.b)$$

$$\varepsilon_{cc} = \varepsilon_c = 0.94 \times 10^{-3} (f_c' (MPa))^{0.25}$$

Figure 4 shows σ - ε curves obtained with the Sakino and Sun model in a 5 ksi strength concrete that is confined by circular and rectangular steel tubes with 50 and 100 width-to-thickness ratios (D/t , b/t). As shown in this figure, confinement improves strength and ductility in circular CFTs and just ductility in rectangular CFTs.

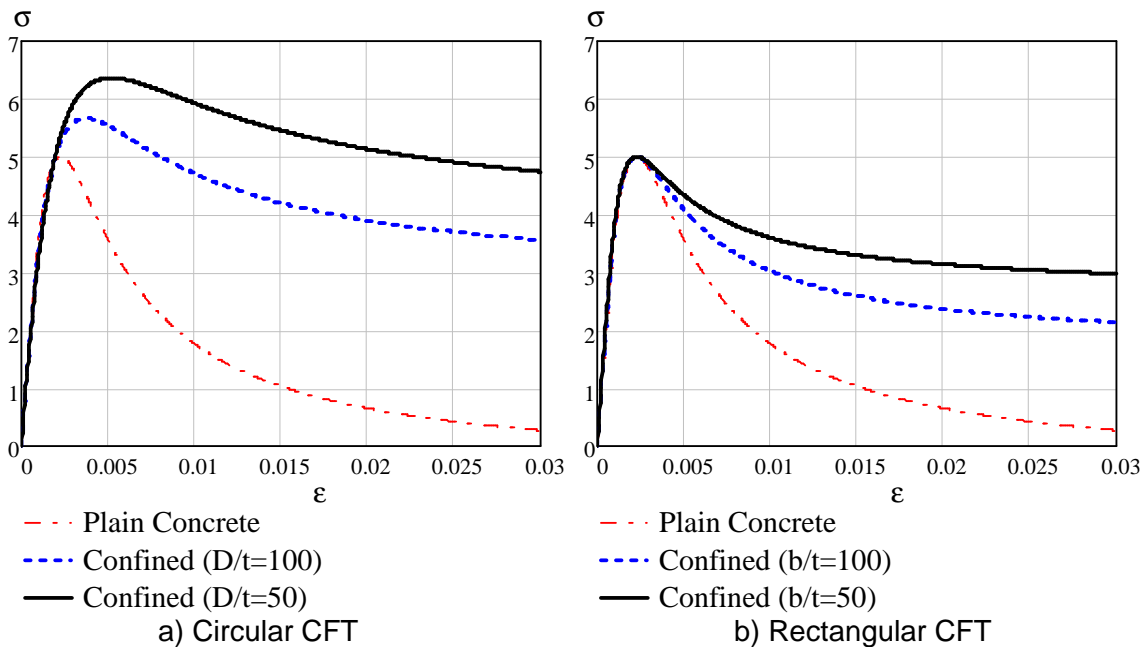


Figure 4. Stress-strain (σ - ε) curves obtained from the Sakino and Sun model for a 5 ksi strength concrete confined by a steel tube with different width-to-thickness ratios.

Conversely, steel tubes can be modeled through an unsymmetrical σ - ε curve to satisfy the Von Mises yield criteria with biaxial stresses. Depending on the b/t ratio, local buckling in rectangular tubes can be handled by a descending branch of the σ - ε curve at a critical strain (ε_{lb}). A careful calibration of the experimental data is needed to obtain the strain ε_{lb} when local buckling takes place. This model postulates that ε_{lb} in circular tubes is reached at high values of strain, and therefore, local buckling effects can be neglected; this approach is tied to the Japanese design requirements for b/t ratios which basically preclude this failure mode.

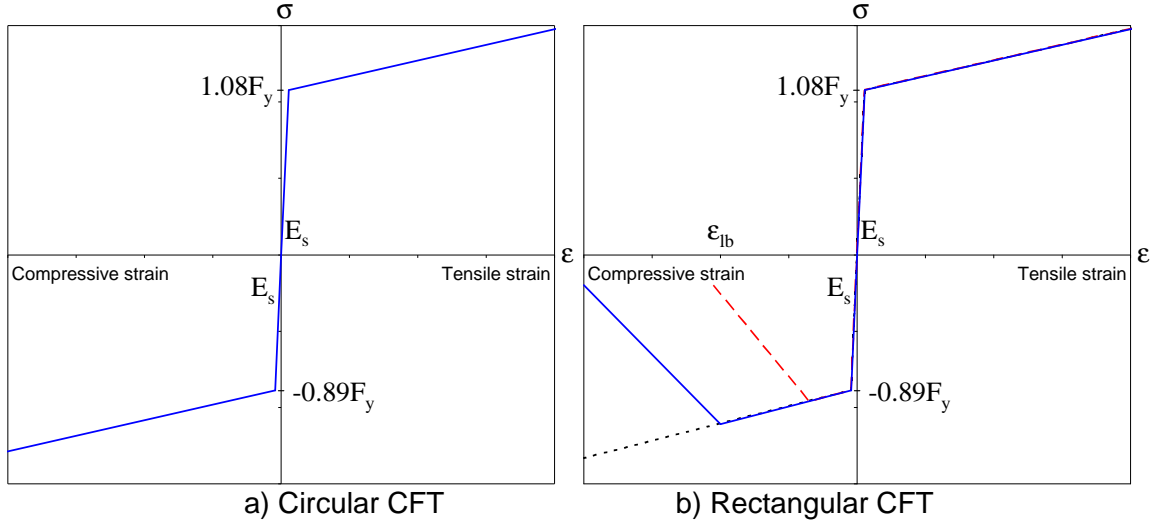


Figure 5. Stress-strain (σ - ϵ) for the steel tubes used with the Sakino and Sun's model

Fiber analysis

As originally described, this study intends to obtain the best prediction in the strength and ductility of a set of large full-scale circular and rectangular CFT beam-columns. The results shown in this section correspond to the following specimens.

1) CCFT20x0.25-5ksi, which is a circular CFT cross section integrated by an HSS20x0.25 steel tube (A500 Gr. B, $R_y=1.4$, $F_y=42$ ksi, $R_u=1.3$, $F_u=58$ ksi) filled with 5 ksi strength concrete. The D/t ratio of this section is 86.0, which is approaching the limit permitted for design in the 2005 AISC specification and 2005 AISC seismic provisions ($D/t=0.15E_s/F_y=103.6$), and well beyond that proposed for the 2010 AISC seismic provisions ($D/t=0.075E_s/F_y=51.8$).

2) RCFT20x12x0.3125-5ksi, which is a rectangular CFT cross section integrated by an HSS20x12x0.3125 steel tube (A500 Gr. B, $R_y=1.4$, $F_y=46$ ksi, $R_u=1.3$, $F_u=58$ ksi) filled with 5 ksi strength concrete. Similarly, the section b/t ratio is 65.7, which is higher than the limits in the 2005 AISC specification ($b/t=2.26\sqrt{(E_s/F_y)}=56.7$) and the one proposed for the 2005 AISC seismic provisions ($b/t=\sqrt{(2E_s/F_y)}=35.5$).

The uniaxial σ - ϵ models used for concrete in the fiber analysis technique are show in the Figure 6 and summarized in the Table 2 and Table 3. The confined concrete strength (f_{cc}) provided by the tubes were obtained with the equation stated in 3.b.

Table 2. Concrete parameters used in the CCFT20x0.25-5ksi specimen

Model	Peak strength		Ultimate strength	
	Stress	Strain	Stress	Strain
EPP-0.95 f_c'	0.95 f_c' =4.75 ksi	0.95 $f_c'/E_c=0.0012$	0.95 f_c' =4.75 ksi	NA
Kent-Park	$f_{cc}'=6.1$ ksi	$\epsilon_{cc}=0.0054$	$f_{cr}=0.6f_{cc}'=3.6$ ksi	$\epsilon_{cr}=9\epsilon_{cc}=0.049$
Popovics	$f_{cc}'=6.1$ ksi	$\epsilon_{cc}=0.0054$	NA	$\epsilon_{cu}=9\epsilon_{cc}=0.049$
Sakino-Sun	$f_{cc}'=6.1$ ksi	$\epsilon_{cc}=0.0053$	NA	NA
EPP-0.95 f_{cc}'	0.95 $f_{cc}'=5.78$ ksi	0.95 $f_{cc}'/E_c=0.0015$	0.95 $f_{cc}'=5.78$ ksi	NA

Table 3. Concrete parameters used in the RCFT20x12x0.3125-5ksi specimen

Model	Peak strength		Ultimate strength	
	Stress	Strain	Stress	Strain
EPP-0.85 f_c'	0.85 f_c' =4.25 ksi	0.85 f_c'/E_c =0.0011	0.85 f_c' =4.25 ksi	NA
Kent-Park	f_c' =5.0 ksi	$\epsilon_c=2f_c'/E_c$ =0.0026	$f_{cr}=0.4f_{cc}'=2.0$ ksi	$\epsilon_{cr}=9\epsilon_c=0.0234$
Popovics	f_c' =5.0 ksi	$\epsilon_c=2f_c'/E_c$ =0.0026	NA	$\epsilon_{cu}=9\epsilon_c=0.0234$
Sakino-Sun	f_c' =5.0 ksi	$\epsilon_c=2f_c'/E_c$ =0.0026	NA	NA

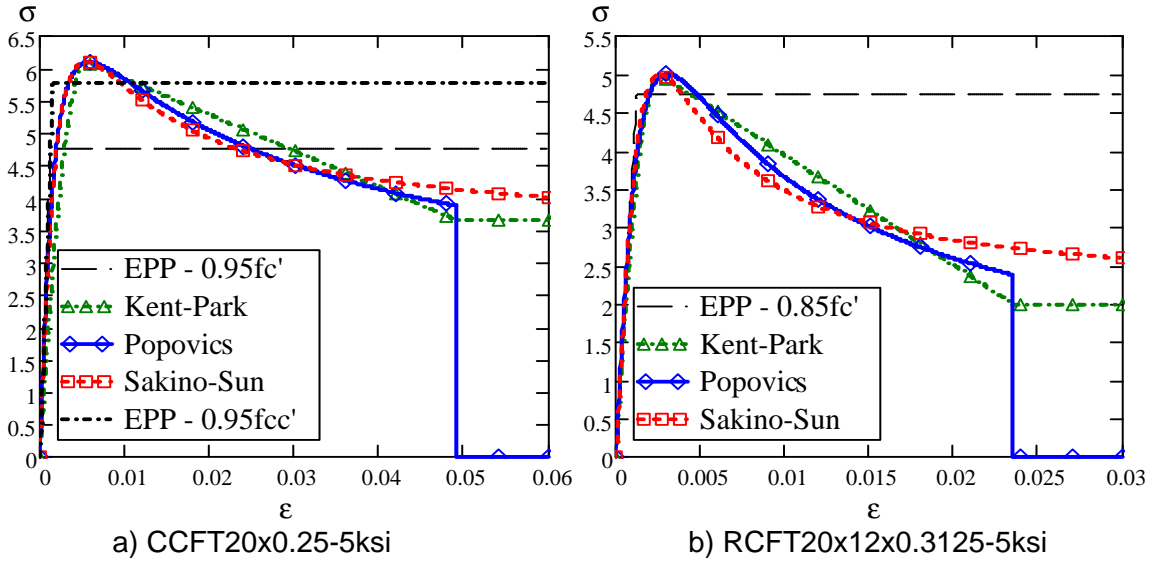


Figure 6. Uniaxial σ - ϵ models used in the concrete fibers

On the other hand, the steel was modeled with an unsymmetrical elastoplastic σ - ϵ with hardening effects (EPH) as described in Figure 5, except when the concrete was assumed elastic-perfectly-plastic (EPP) in which the steel was assumed as well symmetric EPP (Table 4). The overstrength ratios of the nominal yield stress ($R_y=1.4$) and ultimate stress ($R_u=1.3$) were adopted from the AISC seismic provisions (2005). Note that in the elastoplastic with hardening model (EPH) for the RCFTs, a local buckling strain (ϵ_{lb}) was assumed equal to 25 times de compressive yielding strain (ϵ_{yc}); this assumption will be validated and calibrated experimentally in the future.

Table 4. Steel parameters used in the fiber analysis

Specimen \rightarrow	CCFT20x0.25-5ksi		RCFT20x12x0.3125-5ksi	
	EPP	EPH	EPP	EPH
Tensile ultimate σ_u	$R_u F_u=75.4$ ksi	$1.08R_u F_u=81.4$ ksi	$R_u F_u=75.4$ ksi	$1.08R_u F_u=81.4$ ksi
Tensile ultimate ϵ_u	$100\epsilon_y=0.20$	$100\epsilon_y=0.22$	$100\epsilon_y=0.22$	$100\epsilon_y=0.24$
Tensile yield σ_y	$R_y F_y=58.8$ ksi	$1.08R_y F_y=63.5$ ksi	$R_y F_y=64.4$ ksi	$1.08R_y F_y=69.6$ ksi
Tensile yield ϵ_y	$R_y F_y/E_s=0.002$	$1.08R_y F_y/E_s=0.0022$	$R_y F_y/E_s=0.0022$	$1.08R_y F_y/E_s=0.0024$
Comp. yield σ_{yc}	$R_y F_y=-58.8$ ksi	$0.89R_y F_y=-52.3$ ksi	$R_y F_y=-64.4$ ksi	$0.89R_y F_y=-57.3$ ksi
Comp. yield ϵ_{yc}	$R_y F_y/E_s=-0.002$	$0.89R_y F_y/E_s=-0.0018$	$R_y F_y/E_s=-0.0022$	$0.89R_y F_y/E_s=-0.002$
Local buckling strain	NA	NA	NA	$\epsilon_{lb}=80\epsilon_{yc}=-0.16$
Comp. ultimate σ_{uc}	$R_u F_u=-75.4$ ksi	$0.89R_u F_u=-67.1$ ksi	$R_u F_u=-75.4$ ksi	NA
Comp. ultimate ϵ_{uc}	$100\epsilon_{yc}=-0.20$	$100\epsilon_{yc}=-0.18$	$100\epsilon_{yc}=-0.22$	NA

Moment-curvature of the cross-section

Figure 7 shows, for the postulated uniaxial σ - ϵ models, the monotonic and cyclic moment-curvature (M/M_o vs. ϕ) results obtained for the circular CFT cross-section with an initial compression $P=0.2P_o$. In this figure, M_o is the pure bending strength (point B in AISC-05), and P_o is the pure compression strength (point A in AISC-05); As observed, there are low differences regarding the moment strength (EPP $M_{max}=1.24M_o$ vs. others $M_{max}=1.34M_o$), but very different curvature ductility and both strength and stiffness degradation. Monotonic and envelope cyclic differences at high curvatures are caused by the degradation model proposed by Karsan and Jirsa (Makena and Fenves, 1999) that is implemented in the OpenSees software when unloading and reloading cyclically.

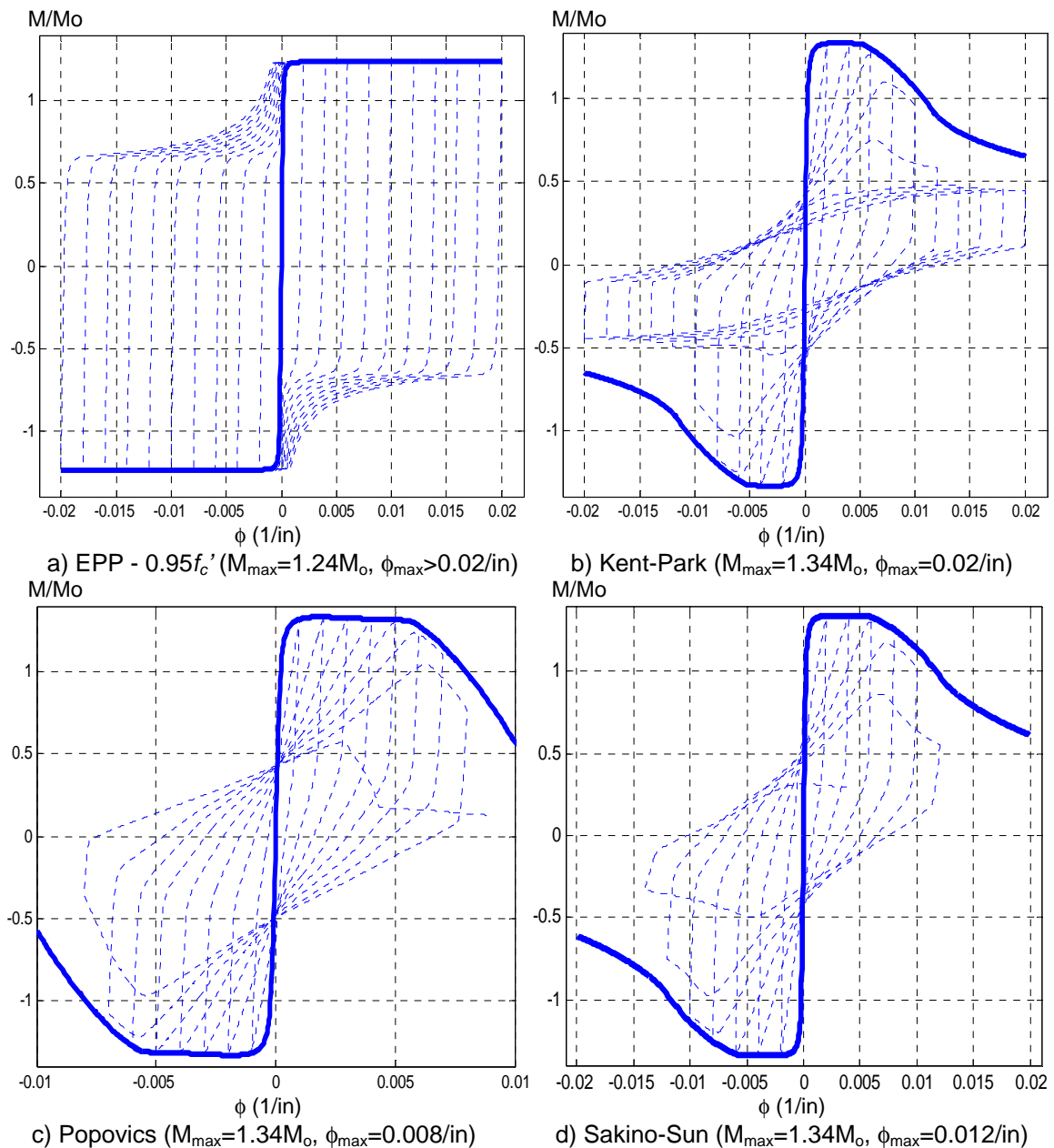


Figure 7. Monotonic (bolted) and cyclic (dashed) M - ϕ curves for the CCFT20x0.25-5ksi cross-section with constant compression force $P=0.2P_o$.

P-M interaction diagrams of the cross-section

The P-M interaction diagram is, by definition, the curve or surface outlined by the axial load and bending moment associated to a desired target (strain, curvature, maximum strength, etc.). In reinforced concrete members, this target is generally defined in terms of the maximum concrete compressive strain, which is usually taken as $\epsilon_c=0.003$ for unconfined concrete. This target intends in reality to capture the maximum cross-section strength, which can also be directly taken from the M- ϕ curves.

Based on a maximum strength target from M- ϕ curves, Figure 9 shows the P-M interaction surfaces for both proposed CFT cross-sections. The strength obtained with the fully-plastic stress distribution equations (as stated in the AISC Design Examples, 2005, points A to E), is also illustrated in this figure. As noticed in this figure, AISC equations (which are based on the fully-plastic stress distribution) have a good prediction of what is expected based on the strain distribution approach with complex uniaxial $\sigma-\epsilon$ models.

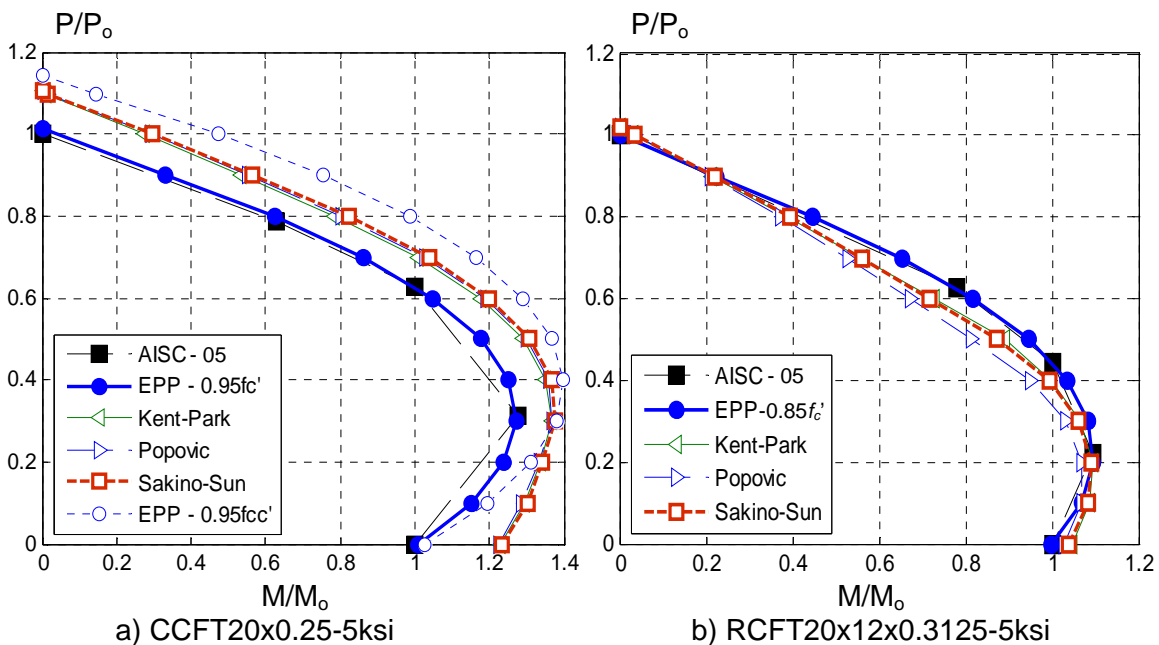
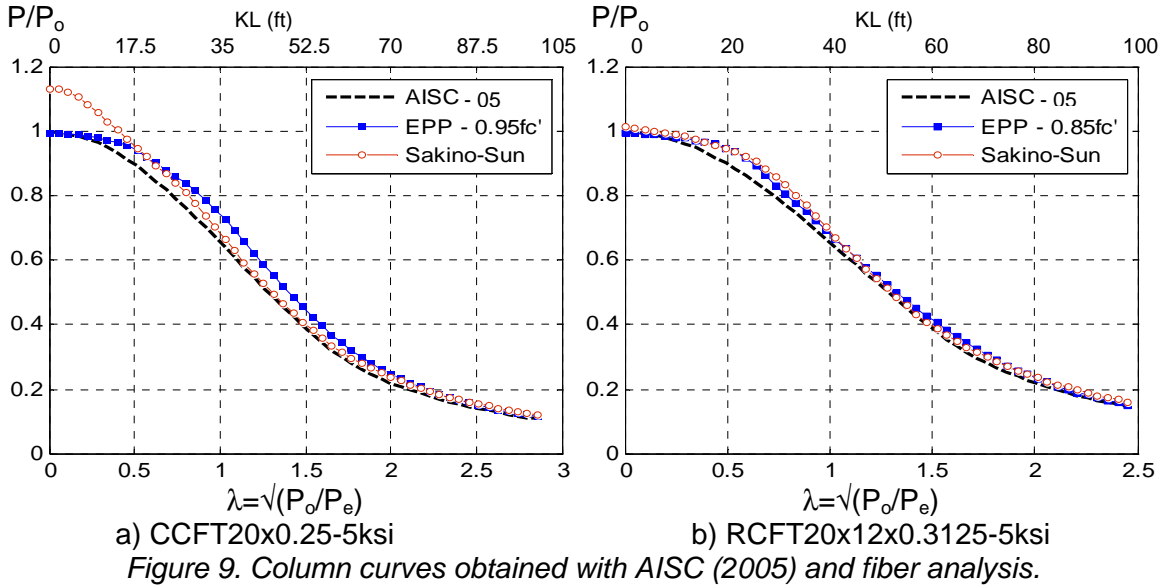


Figure 8. P-M interaction diagrams for the CFT cross-sections with different $\sigma-\epsilon$ models.

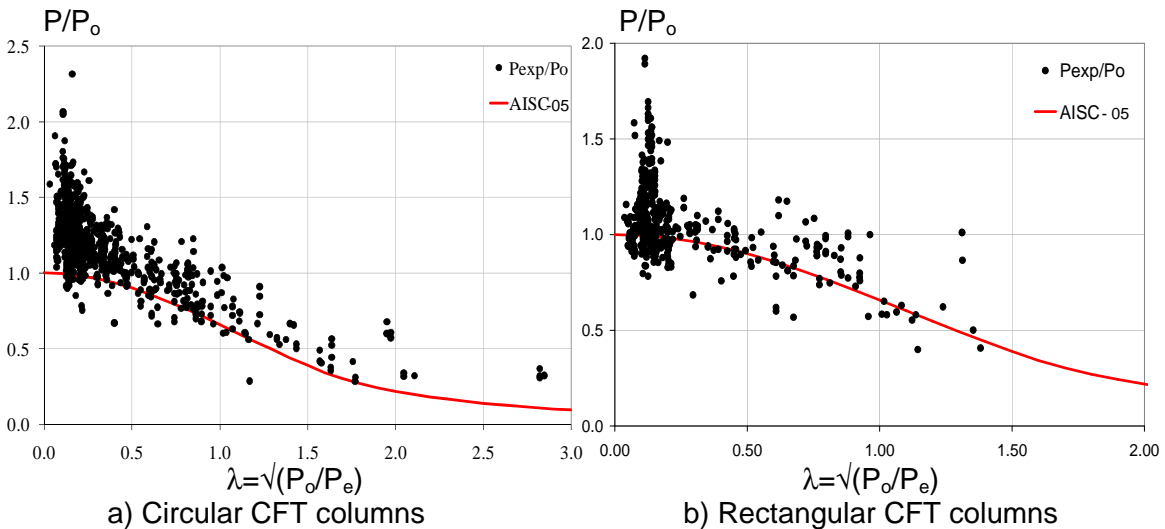
Column curves

Stability effects can be only captured modeling the length, initial imperfections, and a good discretization of the frame elements such that more integration points allow that both P- Δ and p- δ second order effects are considered. Figure 9 shows the results for columns with both circular and rectangular CFT cross-sections, and obtained from the fiber analyses and AISC-05. These curves highlight the benefits of composite columns, with an inelastic buckling range ($\lambda < 1.5$) that includes columns with effective lengths (KL) up to 52.5 ft in the CCFT and 60 ft in the RCFT. Besides, note that fiber analysis results predicted Euler behavior ($\lambda > 1.5$), which is reduced by a 0.877 factor in the AISC specifications to account for geometric imperfection effects. Small differences between AISC and fiber analysis with EPP are due to residual stresses in the structural steel, which are implicitly in AISC but neglected in the fiber-based results.



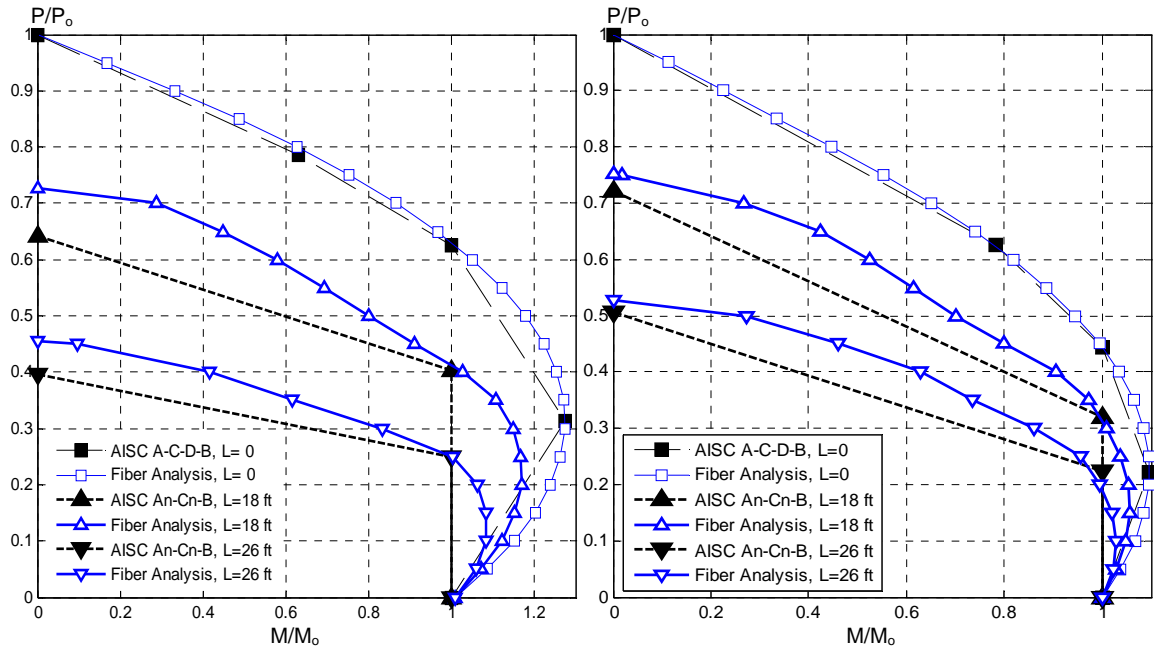
According with the CCFT results, Sakino-Sun model exhibits (due to the f_{cc}' parameter in CCFTs only) a higher strength for short columns (about $\lambda < 0.5$, $KL = 17.5$ ft, $KL/D = 10.5$), which concurred somehow with the European EC-4-2004 ($\lambda = 0.5$) and Japanese AIJ-2001 ($KL/D = 12$) code limits regarding the allowed overstrength due to confinement effects in circular CFT columns; AISC-05 uses the 0.95 factor in the concrete strength ($0.95f_c'$) to account for this confinement effects.

This overstrength is as well exhibited in experimental results. Figure 10 illustrates the maximum compression strength obtained experimentally (P_{exp}) in composite CFT columns, which is normalized with the pure compression strength (P_0) and plotted vs. the slender parameter (λ) as specified in the 2005 AISC specification; The AISC-05 column curve is also plotted in this figure. These empirical results were obtained from databases collected by Aho and Leon (1997), Kim and Leon (2005), and Goode (2007). As observed in this figure, the overstrength is highly impacting short columns mainly in both circular and rectangular CFT columns, with high dispersion though.



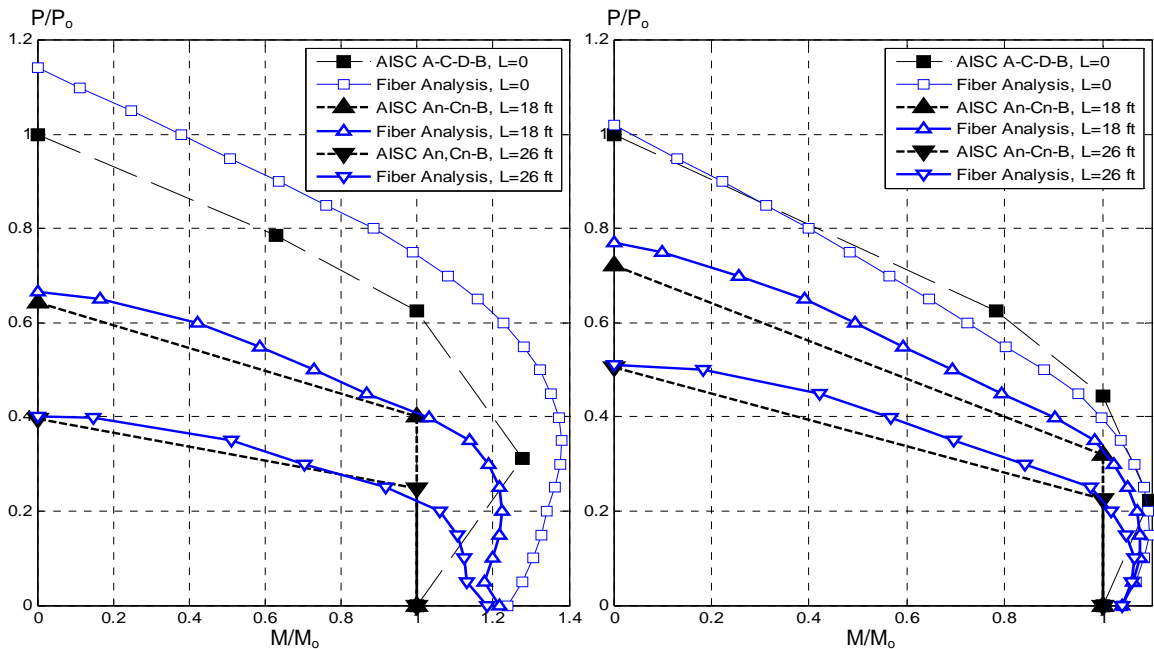
P-M interaction diagrams of the beam-column elements

Figure 11 illustrates the beam-column P-M interaction diagrams obtained with fiber analysis for the EPP and Sakino-Sun models. The postulated beam columns have the previously described circular and rectangular CFT cross sections, lengths of $L=18$ ft and $L=26$ ft, fixed-free boundary conditions ($K=2$), and $L/500$ initial out of plumbness. The corresponding AISC simplified bilinear P-M diagram (AISC A_n-C_n-B) proposed for slender beam-columns, as well as the cross-section strength based on fiber analysis and the 2005 AISC specification (AISC A-C-D-B) are also compared in this figure.



a) CCFT20x0.25-5ksi, EPP model

b) RCFT20x12x0.3125-5ksi, EPP model



c) CCFT20x0.25-5ksi, Sakino-Sun model

d) RCFT20x12x0.3125-5ksi, Sakino-Sun model

Figure 11. P-M interaction diagrams for the composite CFT beam columns

According to these results, AISC simplified bilinear interaction surface is a conservative lower bound of the maximum expected flexural-compressive strength. Note again that confinement induces higher compressive and flexural strength at the cross-section level and short beam-columns ($\lambda < 0.5$), but such compressive overstrength vanished for intermediate beam-columns ($0.5 < \lambda < 1.5$) and long beam-columns ($\lambda > 1.5$).

Lateral force-displacement curves

Expected lateral force (F) vs. the lateral drift (Δ/L) obtained from the fiber analysis using Sakino-Sun model on the postulated CFT beam-columns are shown in Figure 12; these beam-columns have an initial L/500 out-of-plumbness, $0.2P_o$ constant axial compression force, and then they are subjected to cyclic lateral displacement (Δ) with a 1% drift (Δ/L) increment. As a consequence of the local buckling degradation beyond the strain ϵ_{lb} modeled in the RCFT tubes, the displacement ductility is lower than that obtained in the CCFT beam-columns. However, as mentioned before, the definition of the strain at local buckling was assumed without an experimental calibration and, since this parameter is very sensitive in the final ductility, this variable may change accordingly.

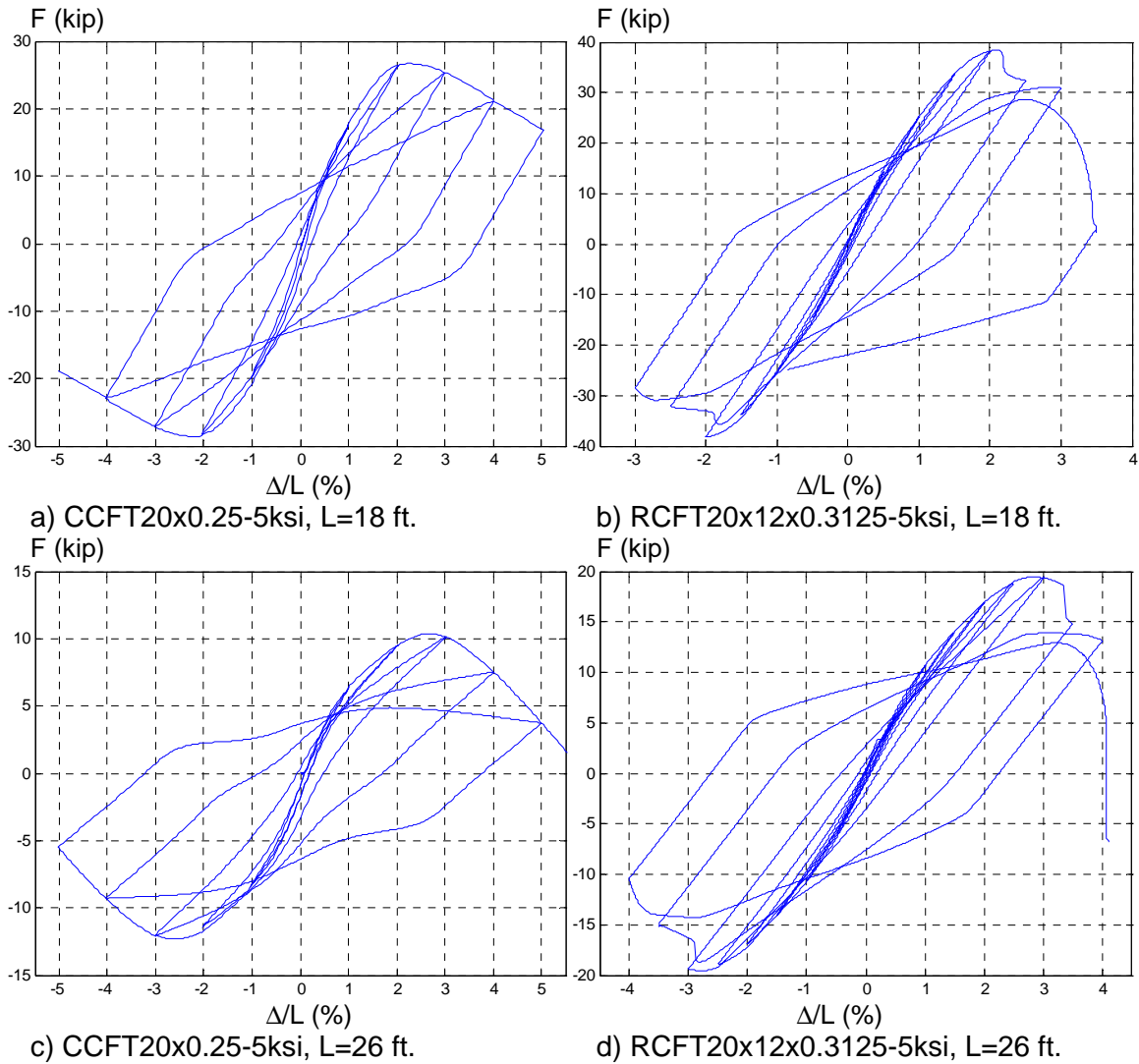


Figure 12. Expected lateral force (F) vs. the lateral drift (Δ/L) using Sakino-Sun model

Conclusions

The benefits on the fiber element analysis technique were briefly described. Based on this technique, some results were obtained and shown emphasizing some issues in the structural behavior of composite cross-sections and composite beam-column elements, such as the effects due to the compressive force, material nonlinearity (stress-strain model), concrete confinement, steel local buckling, triaxial stresses, initial imperfection and geometric nonlinearity effects. Fiber-based analytical results were also compared with those obtained with the AISC (2005) Specification.

As described previously, fiber analysis is a very useful technique to predict the overall behavior of composite beam-column elements. However, the accuracy on the results is highly dependable on the stress-strain model coupled to the fiber cross-section. Simple stress-strain models predict reasonably the ultimate strength; however, more complex material models should be assumed to predict ductility and high displacements such that damage is considered. On the other hand, most of the nonlinearity sources (like strength/stiffness degradation, confinement, local buckling and triaxial stresses effects) have to be calibrated with experimental results and/or more complex analytical techniques in order to incorporate them later on in the uniaxial stress-strain used in the fiber-based model.

More complex techniques, like 3D finite element analysis, can deal with these sources in a straightforward manner. Definition of contact surfaces between concrete and steel can consider a more realistic interaction within these materials; therefore, confinement, local buckling and triaxial stresses can be directly integrated in the behavior (with no influence on the material model). More computing resources and time will be required though.

References

- Aho, M. and Leon, R. (1997), "A database for encased and concrete-filled columns", Master Thesis, School of Civil and Environmental Engineering, Georgia Institute of Technology, Atlanta, Georgia.
- AISC (2005), "Specifications for structural steel buildings". ANSI/AISC 360-05. Chicago, IL, USA.
- AISC Commentary (2005), "Commentary on the specifications for structural steel buildings". AISC. Chicago, IL, USA.
- AISC Design Examples (2005), "Design examples. Version 13.0", CD-ROM included in the Steel Construction AISC Manual. AISC. Chicago, IL, USA.
- AISC Seismic Manual (2005), "Seismic Provisions for structural steel buildings". ANSI/AISC 341-05. Chicago, IL, USA.
- Aval, S. Saadeghvaziri, M. and Golafshani, A. (2002). "Comprehensive composite inelastic fiber element for cyclic analysis of concrete-filled steel tube columns". *Journal of Engineering Mechanics*, Vol. 128, No. 4, ASCE, ISSN 0733-9399. pp. 428-437.
- Choi, Y. Foutch, D. LaFave, J. (2006). "New approach to AISC P–M interaction curve for square concrete filled tube (CFT) beam–columns". *Journal of Engineering Structures*. Vol. 28. pp. 1586–1598.
- Elnashai, A. and Elghazouli, A. (1993). "Performance of composite steel/concrete members under earthquake loading. Part I: analytical model". *Journal of Earthquake Engineering and Structural Dynamics*. Vol. 22, pp. 315-345.
- El-Tawil, S. and Deierlein, G. (1999). "Strength and ductility of concrete encased composite columns". *Journal of Structural Engineering*, Vol. 125, No. 9, September, 1999. ASCE, ISSN 0733-9445/99/1009–1019. Paper No. 19768.

- Goode C. (2007), "ASCCS database of concrete-filled steel tube columns". ASCCS, <http://web.ukonline.co.uk/asccs2/>
- Hajjar, J. and Gourley, B. (1996). "Representation of concrete-filled steel tube cross-section strength". *Journal of Structural Engineering*. Vol. 122, No. 11. pp. 1327–36.
- Hajjar, J. Schiller, P. and Molodan, A. (1998). "A distributed plasticity model for concrete-filled steel tube beam-columns with interlayer slip" *J. of Engineering Structures*, Vol. 20, No. 8, pp. 663–676.
- Izzuddin, B. Karayannis, C. and Elnashai, A. (1993). "Advanced nonlinear formulation for reinforced concrete beam-columns". *Journal of Structural Engineering*. ASCE. Vol. 120. No. 10. pp. 2913-2934.
- Kim, D. and Leon, R. (2005), "A database for composite columns", Master Thesis, School of Civil and Environmental Engineering, Georgia Institute of Technology, Atlanta, Georgia.
- Kim, J. and Kim, T. (2006). "Seismic performance of in-filled steel-concrete composite columns using fiber analysis method". *Journal of Key Engineering Materials*. Vol. 326-328. pp 1821-1824.
- Liang, Q. (2008). "Nonlinear analysis of short concrete-filled steel tubular beam-columns under axial load and biaxial bending". *Journal of Constructional Steel Research*. Vol. 64. pp. 295–304.
- Liew, R. and Chen, H. (2004). "Explosion and Fire Analysis of Steel Frames Using Fiber Element Approach". *J. of Structural Engineering*, Vol. 130, No. 7, ASCE, ISSN 0733-9445. pp. 991-1000.
- Lu, F.W. Li, S.P. and Sun, G. (2006). "A study on the behavior of eccentrically compressed square concrete-filled steel tube columns". *Journal of Constructional Steel Research*.
- McKenna, F. and Fenves, G. (1999) "Open system for earthquake engineering simulation: OpenSees version 1.7.0". Pacific Earthquake Engineering Research Center. University of California, Berkeley.
- Nishiyama, I. Morino, S. Sakino, K. Nakahara, H. Fujimoto, T. Mukai, A. Inai, E. Kai, M. Tokinoya, H. Fukumoto, T. Mori, K. Yoshioka, K. Mori, O. Yonezawa, K. Uchikoshi, M. and Hayashi, Y. (2002), "Summary of research on concrete-filled structural tube column system carried out under the US-Japan cooperative research program on composite and hybrid structures". Building Research Institute (BRI), Report No. 147. ISSN 0453-4972.
- Park, R. and Pauley, T. (1975). "Reinforced concrete structures". Wiley-Interscience. ISBN 0-471-65917-7. pp. 11-47. USA.
- Ricles, J. and Paboojian, S. (1994). "Seismic performance of steel-encased composite columns". *J. of Structural Engineering*, Vol. 120, No. 8, ISSN 0733-9445. Paper No. 6828. pp. 2474-2494.
- Roik, K. and Bergmann, R. (1992), "Composite columns". *Constructional steel design*. Dowling, P. Harding, J. and Bjorhovde, R. (eds.). Elsevier Sc. Publ. ISBN 1-85166-895-0. New York. pp. 443–470.
- Spacone, E. and Filippou, F. (1995). "A fiber beam element for nonlinear dynamic analysis of reinforced concrete structures". *Proceedings of the 10th Conference, Engineering Mechanics*, University of Colorado at Boulder, Colorado, pp. 818-821.
- Taucer, F. Spacone, E. and Filippou, F. (1991). "A fiber beam-column element for seismic response analysis of reinforced concrete structures". Report No. UCB/EERC-91/17, College of Engineering, University of California at Berkeley.
- Tomii, M. and Sakino, K. (1979). "Elastoplastic behavior of concrete filled square steel tubular beam-columns". *Architectural Institute of Japan*. Vol. 280. pp. 111–20.
- Tort, C. and Hajjar, J. (2007). "Reliability-based performance-based design of rectangular concrete-filled steel tube (RCFT) members and frames". *Structural Engineering Report No. ST-07-1*. University of Minnesota. Department of Civil Engineering. Minneapolis, MN.
- Varma, A. Ricles, J. Sauce, R. and Wu Lu, L. (2004), "Seismic behavior and design of high-strength square concrete-filled steel tube beam columns". *J. of Structural Engin.* Vol. 130, No. 2, pp. 169-179.
- White, D. (1986). "Material and geometric nonlinear analysis of local planar behavior in steel frames using interactive computer graphics". Report No. 86-4. Cornell University, Dep. of Struct. Engineering.